JPhys Energy

PAPER • OPEN ACCESS

Screen-printed bismuth telluride nanostructured composites for flexible thermoelectric applications

To cite this article: A Amin *et al* 2022 *J. Phys. Energy* **4** 024003

Journal of Physics: Energy

PAPER

Screen-printed bismuth telluride nanostructured composites for flexible thermoelectric applications

A Amin[1], R Huang[2], D Newbrook[2], V Sethi[2], S Yong[2], S Beeby[2] and I Nandhakumar[1,*]

[1] Department of Chemistry, University of Southampton, Southampton, United Kingdom
[2] Electronics and Computer Science, University of Southampton, Southampton, United Kingdom
* Author to whom any correspondence should be addressed.

E-mail: iris@soton.ac.uk

Keywords: screen-printing, thermoelectrics, bismuth telluride nanowires

Supplementary material for this article is available online

OPEN ACCESS

RECEIVED
4 January 2022

REVISED
8 February 2022

ACCEPTED FOR PUBLICATION
21 February 2022

PUBLISHED
30 March 2022

Abstract

We herein report the results of a facile two-step surfactant assisted reflux synthesis of bismuth telluride (Bi_2Te_3) nanowires (NWs). The as-synthesised NWs had diameters ranging from 70 to 110 nm with a length varying between 0.4 and 3 μm and a preferential lattice orientation of (0 1 5) as determined by grazing incidence x-ray diffraction. We demonstrate for the first time that a solvent/binder paste formulation of *N*-methyl-2-pyrrolidone/polyvinylidene fluoride (PVDF) is suitable for screen-printing the Bi_2Te_3 NWs with the potential for the fabrication of flexible thermoelectric (TE) materials. The wt% of PVDF in the composite films was varied from 10% to 20% to identify the optimal composition with a view to achieving maximum film flexibility whilst retaining the best TE performance. The films were screen-printed onto Kapton substrates and subjected to a post-printing annealing process to improve TE performance. The annealed and screen printed Bi_2Te_3/PVDF NW composites yielded a maximum Seebeck coefficient -192 μV K^{-1} with a power factor of 34 μW m^{-1} K^{-2} at 225 K. The flexible screen printed composite films were flexible and found to be intact even after 2000 bending cycles.

1. Introduction

Thermoelectric generators (TEGs) have the ability to generate electricity from thermal waste heat based on the Seebeck effect and can hence contribute to the sustainability agenda. At present commercial TEGs are made from diced ingots of n-type and p-type semiconductors such as bismuth chalcogenide alloys, which are soldered in series onto metal contacts attached to ceramic sheets [1]. They have so far only been operating in niche fields due to their low efficiency and the bulky, rigid nature of the TEG structure. TEGs however have recently received attention as a potential power source for wearable technologies such as E-textiles as they are safe, long-lasting and maintenance-free with zero-emissions. This involves harvesting energy from the temperature gradient between the body and environment and is hence contingent on the development of high performing flexible TEGs (FTEGs) on curved surfaces. The promise of such FTEG devices is appealing for not only E-textiles but as a power source for sensors and e.g. the internet of things [1–4].

To be suitable for wearable systems the TE materials need to be light-weight with a high degree of mechanical flexibility and be biocompatible and display output powers on the order of a few microwatts per cm^2 [5].

The efficiency of a thermoelectric (TE) material is related to the dimensionless figure of merit (ZT) which is defined as:

$$\mathrm{ZT} = \frac{S^2 \sigma T}{\kappa} \tag{1}$$

Table 1. Table of comparison between our work and previous work on screen-printed flexible n-type Bi_2Te_3 films. It should be noted that most TE screen-printed literature bulk powders and thus have a higher electrical conductivity than the results in this paper.

References	Temperature (K)	Substrate	Active material precursor preparation	Seebeck coefficient (μV K^{-1})	Electrical conductivity (S m^{-1})	Power factor (μW m^{-1} K^{-2})
Our work	225	Kapton	NWs with 10 wt% PVDF	−190	980	36
[17]	300	Kapton	Ball-milled bulk powders of Bi and Te	−134.38	7812.5	141
[18]	300	Kapton	Ball-milled	−137.8	7300	139
[19]	300	Kapton	Ball-milled	−138.4	10 000	192
[20]	288.15	Glass fabric	Ball-milled	−141	67 000	1330
[21]	300	Kapton/aluminium nitride	Ball-milled	−118.2	31 570	441

whereby S represents the Seebeck coefficient determined by the voltage produced by a thermal gradient over a material per degree of temperature, σ is the electrical conductivity, κ is the thermal conductivity and T is the absolute temperature in Kelvin [4]. $S^2\sigma$ is the power factor (PF) which is related to the maximum power that can be delivered to a load, so this parameter must also be optimised for practical systems. The realization of high-performance TE materials therefore requires a high ZT value, which in turn requires a large $S^2\sigma$ and a low κ. In bulk semiconductor materials with high doping, the Wiedemann–Franz rule links σ and κ making it difficult to engineer higher ZT. For low dimensional structures, however, it is possible to decouple some electrical and thermal scattering mechanisms and enhance S and σ through quantum effects to engineer higher ZT values.

Theoretical calculations performed by Dresselhaus *et al* suggested an enhancement of ZT in low dimensional structures such as 1D nanowires (NWs) of Bi_2Te_3 [6, 7] due to phonon scattering at the NW boundaries and an increase in Seebeck coefficient due to the change in the electronic density of states from quantum confinement size effects [6, 8–10]. This has led to renewed interest in the TE field, where surfactant-assisted reflux synthesis has enabled reliable and scalable synthesis of NWs with high yields [11, 12].

Inkjet printing presents a number of challenges that could limit its use for industrial applications such as e.g. a narrow ink viscosity range of between 1 and 30 cP that could be difficult and more costly to maintain within an industrial setting [13–15]. To aid the commercialisation of Bi_2Te_3-based nanomaterials, other printing approaches such as screen-printing should be considered as this approach has been widely used in the fabrication of flexible electronics such as organic light-emitting diodes (OLEDs) and solar cells [16]. This involves spreading a viscous paste of a TE ink through a patterned porous mesh (screen) onto a substrate and forming a wet thick film (thickness >10 μm) [14, 16]. A major advantage of screen-printing over inkjet printing is its wider viscosity range 1000–10 000 cP which allows for a higher degree of ink flexibility.

In the literature ball-milled Bi and Te bulk powders are typically used as active materials in paste formulations [17–21] for screen-printing and the results of these studies are summarised in table 1.

We report the first results of a study in which n-type Bi_2Te_3 NWs were successfully screen-printed onto flexible Kapton substrates from simple paste formulations of polyvinylidene fluoride (PVDF) in *N*-methyl-2-pyrrolidone (NMP). The NMP-PVDF solvent-binder combination was chosen for its wide use in industrial screen-printing [22, 23]. We also demonstrate the suitability of the screen-printed NW composite films for flexible TE applications by performing a bending cycle analysis.

2. Methods

2.1. Experimental methods

To prepare Bi_2Te_3 NWs the synthesis involved dissolving 3.84 g tellurium dioxide (>99%, Aldrich), 1.6 g polyvinylpyrrolidone (K-30, Fluka), 4.83 g potassium hydroxide (Fisher) in 160 ml of ethylene glycol (EG) (Fisher) in a 250 ml round bottom flask (RBF). The RBF was connected to a condenser and connected to a Schlenk line to reduce oxygen exposure during the synthesis. The RBF was placed in a silica oil bath on a magnetic stirrer hot plate and heated to 160 °C for 1 h. The 8 ml of hydrazine hydrate (50%–60%, Sigma Aldrich) was injected into the mixture and heated for a further hour. The 8 g of $Bi(NO_3)_3 \cdot 5H_2O$

(98%, Aldrich) was separately dissolved in 40 ml of EG and then injected into the mixture. After another hour of stirring the RBF was taken out of the oil bath and allowed to cool to room temperature with no stirring applied.

Once cooled, the RBF was taken into a nitrogen-filled glovebox, where the mixture was poured into 16 centrifuge bottles along with 5 ml of acetone (Sigma Aldrich). Methanol (Fisher) was used to retrieve some of the residue from the RBF and subsequently poured into the bottles. The bottles were centrifuged overnight at 5000 rpm and for 2 h at 10 000 rpm, after which the supernatant was decanted. It should be noted that the supernatant still contained NWs, but the quantity was not deemed to be worth extracting. A cleaning solution made of 3:1 acetone and deionised water was added to the bottles. The precipitant NWs are then dispersed in a cleaning solution via bath sonication for 15 min. The dispersions were then mixed via a top mixer at 3000 rpm for 10 s each before they were centrifuged for 20 min at 10 000 rpm. This process was repeated three times to fully clean the NWs, which were then vacuum dried overnight. The resulting NW powder was removed and measured to be ∼6.5 g.

Two pastes were formulated one with 10% and another with 20% concentrations of PVDF with respect to the weight of the screen-printed film. For the 10% and 20% paste, 1.8 and 1.6 g of dried Bi_2Te_3 NW powder were dispersed in 1 and 2 ml of NMP (anhydrous 99.5%, Sigma Aldrich) via 4 h of bath sonication with 1 h stirring at 400 rpm sessions before and after bath sonication. A solution of PVDF (average mol wt% ∼ 534 000, Sigma Aldrich) and NMP solution was made in a nitrogen-filled glovebox by stirring 5 ml of NMP with 1 g of PVDF on a hot plate for 2 h at 60 °C and then at room temperature for 2 d. The 1 and 2 ml of 200 mg ml^{-1} PVDF/NMP were added to 10% and 20% pastes respectively and they were left to stir overnight. The final paste's weight compositions were 44.3%, 4.9% and 50.3% for the 10% paste and 26.1%, 6.5% and 67.3% for the 20% paste, for the Bi_2Te_3 NW powder, PVDF and NMP respectively. Before printing the pastes were further bath sonicated for 4 h then speed mixed for 5 min at 2500 rpm.

Before screen-printing the pastes were further bath sonicated for 4 h and speed mixed at 2500 rpm for 5 min. The pastes were then printed by a screen-printer (DEK-248) using a stainless-steel based 250 mesh screen (MCI precision) onto Kapton substrates. The print gap used was 0.5 mm, with the active mesh area divided into three strips with an area each of 5 × 50 mm for a total active area of 7.5 cm^2. The screen-printed films were finally cured at 140 °C in a vacuum oven for 1 h and left to cool overnight.

The strips were cut into smaller film samples and placed into a tube furnace (CU2006/TF2006, Severn Thermal Solutions). The furnace was purged with Ar at 2 l min^{-1} for 2 h before heating. The samples were heated at a rate of 5 K min^{-1} to their target temperature of 400 °C and then held for 2 h before cooling at a rate of 3 K min^{-1}.

2.2. Characterisation methods

Scanning electron microscopy (SEM) imaging was performed on a field emission scanning electrode microscope (JSM 7500F, JEOL). Images were taken in secondary electron mode using a 5 and 15 kV accelerating voltage. The working distance between the samples and the field emitter source aperture was approximately 6 and 7 mm. To minimise electric charging of the PVDF composites during SEM imaging these were sputter coated with a thin layer of gold.

Energy dispersive x-ray (EDX) measurements were conducted using an SEM (FEI XL30 ESM, Phillips) connected with an EDX detector (Thermo Scientific Ultra Dy 10 mm^2 EDS). Measurements were taken using a 10 kV accelerating voltage. The working distance between the samples and the field emitter source aperture was approximately 10 mm.

Grazing incidence x-ray diffraction (GIXRD) measurements were performed using a Rigaku Smartlab x-ray diffractometer with CuK_α radiation. All samples were scanned from a 2θ of 10°–70° with a step size of 10° min^{-1}. The GIXRD spectra were then analysed in PDXL2 and compared against reference spectra from the International Centre of Diffraction Data (ICDD) database under file ICDD PDF 01-085-0439.

Variable temperature measurements for electrical conductivity, carrier concentration and carrier mobility were acquired on a Hall measurement system (HL5500PC, Nanometrics) from 150 K to 425 K in steps of 25 K under a magnetic field of 0.5 T. The current was calibrated to ensure normal ohmic conduction with maximum voltage signal of 20 mV. The average reading was taken as the result and the standard deviation as the error.

Seebeck measurements were conducted on a commercial Joule Yacht MRS-3L Seebeck measurement system over the temperature range of 150 K–425 K in steps of 25 K. The Seebeck measurements are reported by the manufacturer to have an error of 7%. Samples were mounted between two copper heat reservoirs with gold contacts as both heaters and electrical contacts. The Seebeck coefficient was measured using the differential method with a maximum temperature difference of 10 K by fixing the temperature of one side of

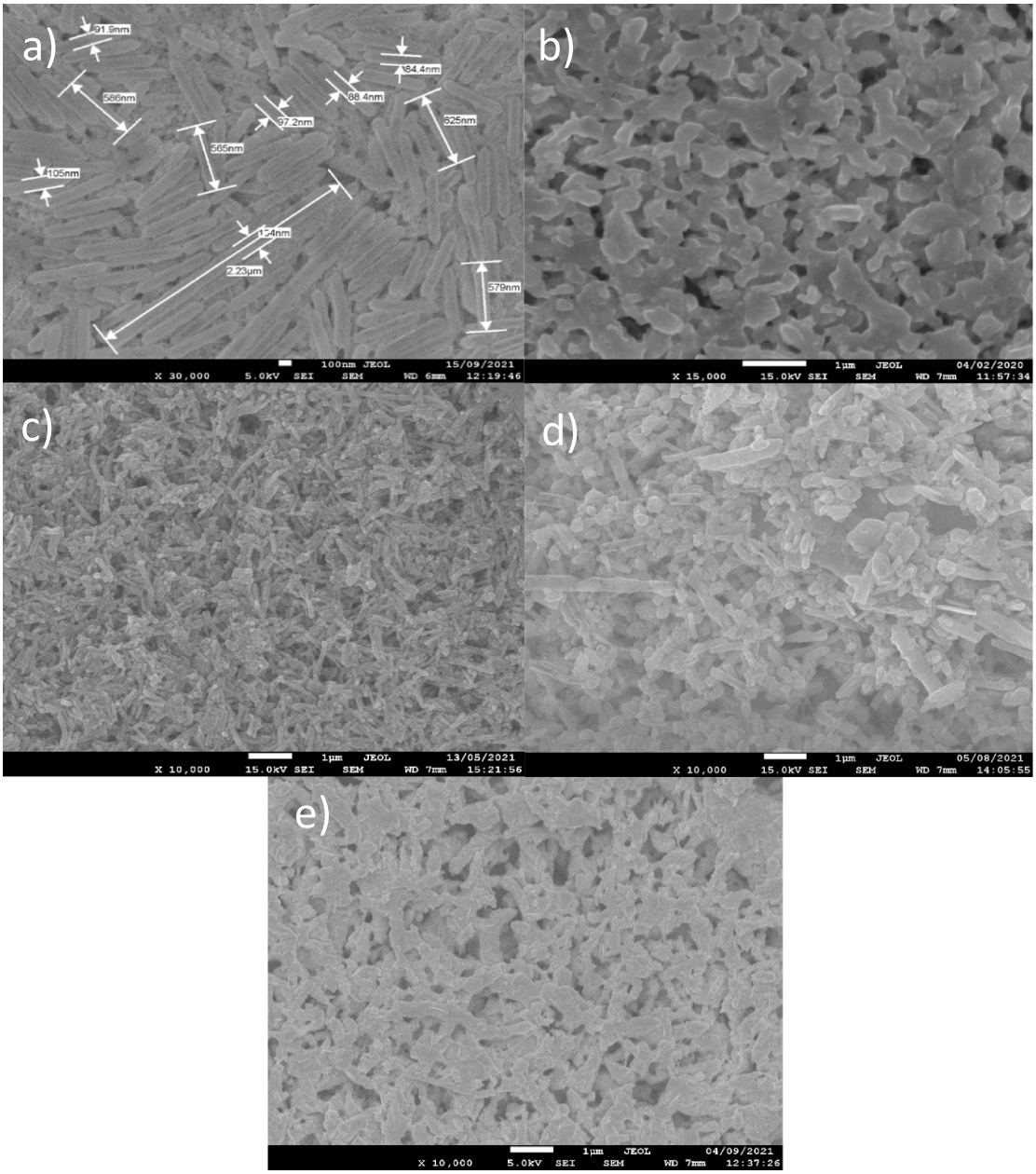

Figure 1. SEM micrographs of (a) unannealed drop-casted Bi_2Te_3 NWs (b) annealed drop-casted Bi_2Te_3 INNs (c) annealed screen-printed 20% PVDF-NWs (d) 10% PVDF-NWs and (e) fully formed 10% PVDF-INNs.

the sample and heating the other side at a constant heating rate and sampling voltage and temperature simultaneously. A linear fitting of potential difference and temperature difference is taken, and the gradient taken as the Seebeck coefficient according to $\mathrm{d}V/\mathrm{d}T = -\alpha$. Nickel foil is regularly used to calibrate and check normal operation of the tool. The Seebeck measurements are reported by the manufacturer to have an error of 7%.

3. Results and discussion

SEM images as depicted in figure 1(a) show the morphology of the as synthesised Bi_2Te_3 NWs. These exhibited diameters ranging from 70 to 110 nm and a length of between 0.4 and 3 μm (cf figure 1(a)). After annealing at 400 °C for 2 h the NWs formed interconnected nanowire networks (INNs) as shown in figure 1(b). The morphology of the 10% PVDF-NW and 20% PVDF-NW nanowire PVDF composite films

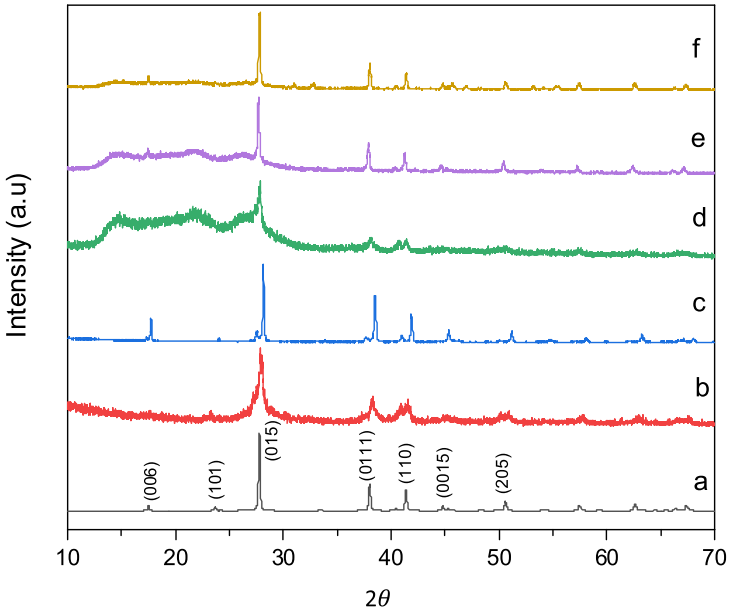

Figure 2. GIXRD diffraction patterns obtained for (a) reference XRD of telluro bismuthite (Bi_2Te_3) mineral from ICDD database (PDF 01-085-0439) (b) unannealed drop-casted Bi_2Te_3 NWs, (c) drop-casted Bi_2Te_3 NWs annealed in an argon atmosphere at 400 °C for 2 h and (d) unannealed screen-printed PVDF/Bi_2Te_3 NW composite film and (e) screen-printed PVDF/Bi_2Te_3 NW composite film annealed in an argon atmosphere at 400 °C for 2 h and (f) screen-printed Bi_2Te_3 INNs films annealed in an argon atmosphere at 400 °C for 2 h.

after annealing (figures 1(c) and (d)) reveals the presence of some NWs that remained intact and also indicates the formation of some INNs and this process seems to be more advanced in the 10 wt% PVDF-NW samples. The morphology difference between the annealed PVDF-NWs and the PVDF-INNs may be attributed to the residual amount of PVDF that is still present within the samples and has not burnt off during the annealing process. The impact of this on fully formed interconnected NW networks was hard to control. Figure 1(e) reveals films composed of 10% PVDF-NW that formed complete INNs referred to as 10% PVDF-INNs. The 400 °C annealing temperature is close to the region where PVDF mass loss occurs as can be seen in the thermogravimetric analysis plot (see supplementary information figure S1 available online at stacks.iop.org/JPEnergy/4/024003/mmedia). It can therefore be expected that the PVDF binder can burn off during the annealing process. Prior to annealing the NWs formed loose electrical contacts leading to poor electrical conductivity. The sintering of the NWs lead to higher electrical conductivities and better TE performance which its most likely due the percolative nature of the interconnected NW networks.

The stoichiometry of the Bi_2Te_3 NWs before annealing was determined by EDX to be Bi ∼36% and Te 64% which is close to stoichiometric Bi_2Te_3. A strong fluorine peak due to the PVDF binder was also detected in EDX that was significantly reduced in its intensity after annealing indicating that the binder has been at least partially removed (see figure S2). GIXRD spectra obtained for the annealed drop-casted as well as screen-printed NWs in the presence and absence of PVDF are shown in figure 2 respectively. These reveal a Bi_2Te_3 crystal structure with a preferential (0 1 5) orientation which is in agreement with previous reports [11]. The standard ICDD PDF card data (01-085-0439) has been used to identify and index all detected peaks. The crystallinity of the Bi_2Te_3 NWs improves upon annealing giving rise to more pronounced peaks in GIXRD. However, the annealing process did not result in any phase or compositional changes. For the screen-printed films, there is a broad peak visible between at 2θ 15°–25°, which may be attributed to the PVDF binder as this is not detectable in the drop-casted pristine Bi_2Te_3 films. Further, this broad peak notably decreased in intensity after annealing illustrating that the PVDF had only been partially removed.

The in-plane Seebeck coefficient, electrical conductivity and PF for the screen-printed composite films were collected over a temperature range of 250 K–425 K range and are shown in figure 3.

All films displayed a negative Seebeck coefficient which is consistent with n-type behaviour. The annealed and screen-printed Bi_2Te_3/PVDF NW composite films displayed a maximum Seebeck coefficient of $-192\ \mu V\ K^{-1}$ with a PF of 36 $\mu W\ m^{-1}\ K^{-2}$ at 225 K and a room temperature Seebeck coefficient and PF of

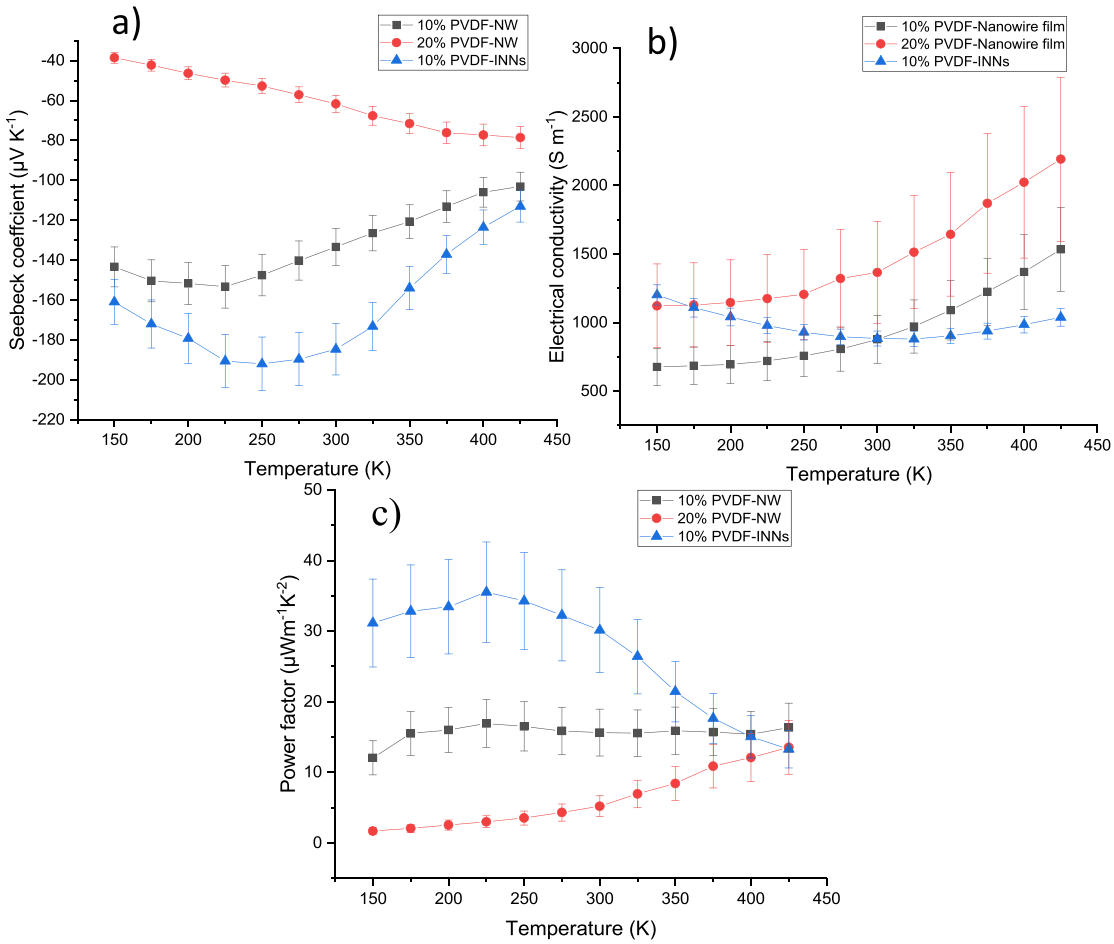

Figure 3. Temperature-dependent TE properties measured over a temperature range of 250 K–425 K for (a) Seebeck coefficient, (b) electrical conductivity and (c) PF of the annealed INN film and screen-printed 10% PVDF-NW, 20% PVDF-NW and 10% PVDF-INNs films. For each data point presented at least three measurements were performed per sample and in total at least ten samples were measured.

$-185\ \mu V\ K^{-1}$ and $30\ \mu W\ m^{-1}\ K^{-2}$ respectively. These values are in good agreement with those reported in studies on flexible and printed composite nanomaterials [24–27]. For example Ou *et al* recently reported a PF of $30\ \mu W\ m^{-1}\ K^{-2}$ for aerosol jet printed nanocrystals of Bi_2Te_3/Sb_2Te_3 embedded within a flexible poly(3,4-ethylenedioxythiophene)polystyrene sulfonate matrix [27]. Compared to ball milled bulk powders of bismuth and tellurium (as summarised in table 1) our reported Seebeck coefficient is higher whilst the PF is lower due to the lower electrical conductivities measured for our NWs thin film composites. If we compare our PFs to a recent study on inkjet printed NWs of bismuth telluride by Chen *et al* our values are comparable. This study in particular reports a maximum PF at room temperature of $\sim 80\ \mu W\ m^{-1}\ K^{-2}$ [28]. The difference in our results is due to the addition of PVDF in order to formulate a screen-printable paste, which does not burnt off completely. This lowers the films carrier mobility and overall electrical conductivity. However, in the case of inkjet printing a high number of printing passes is required in order to achieve sufficient film thickness.

To evaluate the suitability of the NW composite films for flexible TE applications we performed bending tests over 2000 cycles as shown in figure 4 as well as measuring the resistance (R) and Seebeck coefficient as a function of bending radius. The bending tests as a function of bending radius, show that the Seebeck coefficient increases slightly for smaller bending radii. However, the results are within the error range and no significant change can be observed. The film resistance does not change significantly as a function of bending cycle. From these tests, we believe the material to be suitable for wearable flexible electronic applications as after 2000 cycles the film has not delaminated from the substrate.

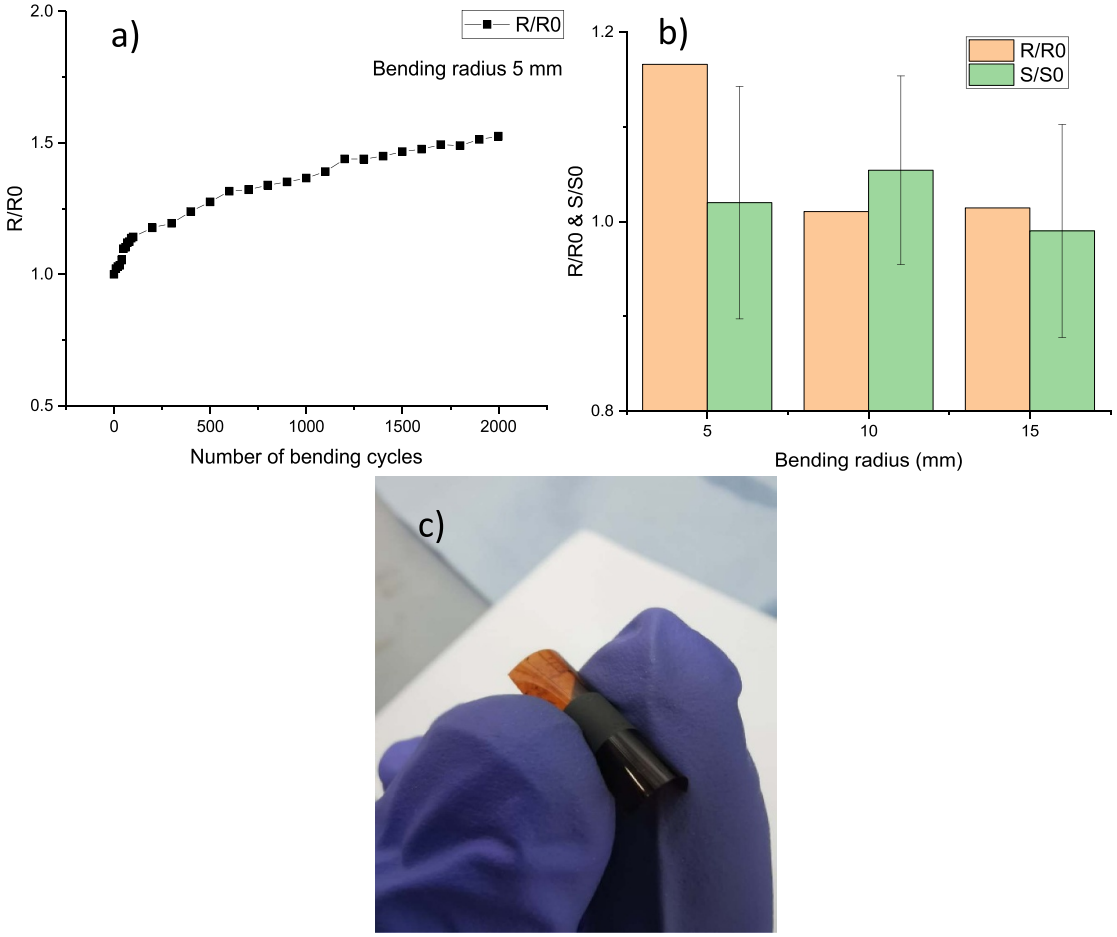

Figure 4. (a) Resistance normalized to initial resistance of 10% PVDF-NW film for 2000 bending cycles, with a bending radius of 5 mm (b) the resistance normalized to initial resistance and Seebeck coefficient normalized to initial Seebeck coefficient for different bending cycles radius and (c) photograph insert of curved composite NW film.

4. Conclusions

We have demonstrated that PVDF is a suitable binder for the screen-printing of flexible Bi_2Te_3 NW films which provides a potential route towards the fabrication of flexible TE materials. The Bi_2Te_3/PVDF composite films exhibited a Seebeck coefficients of $-192\ \mu V\ K^{-1}$ and a PF of $36\ \mu W\ m^{-1}\ K^{-2}$ at 225 K. Further studies are currently ongoing to optimise the TE performance of the composite materials.

Data availability statement

The data that support the findings of this study are available upon reasonable request from the authors.

Acknowledgment

The authors acknowledge the financial support of equipment Grant (EP/K00509X/1) for the SmartLab. A Amin and I Nandhakumar wish to acknowledge the RSC for Grant E21-3692126553 and EPSRC grant EP/T026219/1.

ORCID iDs

D Newbrook https://orcid.org/0000-0002-5047-6168
S Beeby https://orcid.org/0000-0002-0800-1759
I Nandhakumar https://orcid.org/0000-0002-9668-9126

References

[1] Shi X-L, Zou J and Chen Z-G 2020 Advanced thermoelectric design: from materials and structures to devices *Chem. Rev.* **120** 7399–515
[2] Champier D 2017 Thermoelectric generators: a review of applications *Energy Convers. Manage.* **140** 167–81
[3] Wang Y, Shi Y, Mei D and Chen Z 2017 Wearable thermoelectric generator for harvesting heat on the curved human wrist *Appl. Energy* **205** 710–9
[4] Ali Bashir M B, Mohamad M, Said S B M, Sabri M F M, Hamid Elsheikh M, Haji Hassan M and Shnawah D A 2013 A review on thermoelectric renewable energy: principle parameters that affect their performance *Renew. Sustain. Energy Rev.* **30** 337–55
[5] Rong G, Zheng Y and Sawan M 2021 Energy solutions for wearable sensors: a review *Sensors* **21** 1–23
[6] Hicks L D and Dresselhaus M S 1993 Thermoelectric figure of merit of a one-dimensional conductor *Sci. Comput.* **47** 8–11
[7] Hicks L D and Dresselhaus M S 1993 Effect of quantum-well structures on the thermoelectric figure of merit *Phys. Rev.* B **47** 12727–31
[8] Chhatrasal G and Kamal K K 2016 Recent advances in thermoelectric materials *Prog. Mater. Sci.* **83** 330–82
[9] Chen G and Shakouri A 2002 Heat transfer in nanostructures for solid-state energy conversion *J. Heat Transfer* **124** 242–52
[10] Mao J, Liu Z and Ren Z 2016 Size effect in thermoelectric materials *npj Quantum Mater.* **1** 16028
[11] Zhang G, Kirk B, Jauregui L A, Yang H, Xu X, Chen Y P and Wu Y 2012 Rational synthesis of ultrathin n-type Bi_2Te_3 nanowires with enhanced thermoelectric properties *Nano Lett.* **12** 56–60
[12] Wang K, Liang H-W, Yao W-T and Yu S-H 2011 Templating synthesis of uniform Bi_2Te_3 nanowires with high aspect ratio in triethylene glycol (TEG) and their thermoelectric performance *J. Mater. Chem.* **21** 15057–62
[13] Chen B, Das S R, Zheng W, Zhu B, Xu B, Hong S, Sun C, Wang X, Wu Y and Claussen J C 2017 Inkjet printing of single-crystalline Bi_2Te_3 thermoelectric nanowire networks *Adv. Electron. Mater.* **3** 1600524
[14] Boudouris B W and Yee S 2017 Printed thermoelectric materials and devices: fabrication techniques, advantages, and challenges *J. Appl. Polym. Sci.* **134** 44456
[15] Kipphan H 2001 *Handbook of Print Media: Technologies and Production Methods* (Heidelberg: Springer Science & Business Media)
[16] Deganello D 2013 Printing techniques for the fabrication of OLEDs *Organic Light-Emitting Diodes (OLEDs): Materials, Devices and Applications* (Cambridge: Elsevier)
[17] Cao Z, Koukharenko E, Tudor M J, Torah R N and Beeby S P 2016 Flexible screen printed thermoelectric generator with enhanced processes and materials *Sens. Actuators* A **238** 196–206
[18] We J H, Kim S J and Cho B J 2014 Hybrid composite of screen-printed inorganic thermoelectric film and organic conducting polymer for flexible thermoelectric power generator *Energy* **73** 506–12
[19] Cao Z, Tudor M J, Torah R N and Beeby S P 2016 Screen printable flexible BiTe-SbTe-based composite thermoelectric materials on textiles for wearable applications *IEEE Trans. Electron Devices* **63** 4024–30
[20] Kim S J, We J H and Cho B J 2014 A wearable thermoelectric generator fabricated on a glass fabric *Energy Environ. Sci.* **7** 1959–65
[21] Feng J, Zhu W, Zhang Z, Cao L, Yu Y and Deng Y 2020 Enhanced electrical transport properties via defect control for screen-printed Bi_2Te_3 films over a wide temperature range *ACS Appl. Mater. Interfaces* **12** 16630–8
[22] Riley J 2000 *Advances in Electrochemical Science and Engineering* vol **493** (Weinheim: Wiley)
[23] Gören A, Mendes J, Rodrigues H M, Sousa R E, Oliveira J, Hilliou L, Costa C M, Silva M M and Lanceros-Méndez S 2016 High performance screen-printed electrodes prepared by a green solvent approach for lithium-ion batteries *J. Power Sources* **334** 65–77
[24] Chatterjee K, Mitra M, Kargupta K, Ganguly S and Banerjee D 2013 Synthesis, characterization and enhanced thermoelectric performance of structurally ordered cable-like novel polyaniline-bismuth telluride nanocomposite *Nanotechnology* **24** 215703
[25] Jiao F *et al* 2014 Inkjet-printed flexible organic thin-film thermoelectric devices based on p- and ethenetetrathiolates/polymer composites through ball milling *Phil. Trans. R. Soc.* A **372** 201300008
[26] Thongkham W, Lertsatitthanakorn C, Jiramitmongkon K, Tantisantisom K, Boonkoom T, Jitpukdee M, Sinthiptharakoon K, Klamchuen A, Liangruksa M and Khanchaitit P 2019 Self-assembled three-dimensional Bi_2Te_3 nanowire-PEDOT:PSS hybrid nanofilm network for ubiquitous thermoelectrics *ACS Appl. Mater. Interfaces* **11** 6624–33
[27] Ou C, Sangle A L, Datta A, Jing Q, Busolo T, Chalklen T, Narayan V and Kar-Narayan S 2018 Fully printed organic-inorganic nanocomposites for flexible thermoelectric applications *ACS Appl. Mater. Interfaces* **10** 19580–7
[28] Chen B, Kruse M, Xu B, Tutika R, Zheng W, Bartlett M D, Wu Y and Claussen J C 2019 Flexible thermoelectric generators with inkjet-printed bismuth telluride nanowires and liquid metal contacts *Nanoscale* **11** 5222–30